11378 *Inorg. Chem.* **2010**, *49*, 11378–11385
DOI: 10.1021/ic1013126

Inorganic Chemistry
Article

Establishment of Structure-Conductivity Relationship for Tris(2,2′-bipyridine) Ruthenium Ionic C_{60} Salts

Jie Hong, Matthew P. Shores, and C. Michael Elliott*

Department of Chemistry, Colorado State University, Fort Collins, Colorado 80523-1872, United States

Received June 30, 2010

Three ionic C_{60} salts with $[Ru(bpy)_3]^{m+}$ (bpy = 2,2′-bipyridine) as cations were synthesized. The UV−vis−NIR spectra, XPS spectra, and elemental analysis have demonstrated their compositions: $[Ru(bpy)_3]_2(C_{60})$ (**1**), $[Ru(bpy)_3](C_{60})$ (**2**), and $[Ru(bpy)_3](C_{60})_2$ (**3**). Single crystals of polycrystalline compounds **1** and **2** were obtained as solvates. At room temperature, all three salts are semiconducting with the highest four-probe conductivity observed for compound **1** at ∼10 S m^{-1}. The electronic conduction mechanisms can be described appropriately by an electron hopping model in this immobilized polyvalent redox system.

Introduction

In recent years, metal-complex ionic fullerene salts (C_{60}^{n-}) have attracted considerable attention because of their interesting physical and structural properties.[1−11] Transition metal polypyridine complexes, most notably, tris(2,2′-bipyridine)ruthenium, $[Ru(bpy)_3]^{m+}$, have a number of photochemical and electrochemical properties which make them of interest for both fundamental and applied studies.[12] The similarity of electrochemical potentials of $[Ru(bpy)_3]^{m+}$ and C_{60}^{n-} gives rise to the possibility for obtaining new-charge transfer ionic salts $[Ru(bpy)_3^{m+}]_n(C_{60}^{n-})_m$.[8,12,13] In addition, $[Ru(bpy)_3]^{m+}$ has a roughly spherical shape and comparable dimensions to the C_{60} molecule.[14,15] The presence of large cations, $[Ru(bpy)_3]^{m+}$, can effectively break the ball-to-ball close contact experienced in, for example, alkali-metal doped C_{60}, and perhaps allow the formation of classical ionic structures such as rock salts.[13] Besides the alteration of structure, since both cations and anions are redox active[8,12] relative to, for example, superconducting alkali-metal doped C_{60} where only the anions can exchange electrons,[16] the possibility arises for novel electronic properties for the ionic salts. Semiconducting $[Ru(bpy)_3^{2+}](C_{60}^{-})_2$ has been successfully synthesized by Foss et al.[13] This material was reported to have a two-probe conductivity of 1.0 S m^{-1} at 25 °C.[13] However, neither structural information nor detailed discussion about electron conduction was reported.[13] The previous study gave rise to a demand for in-depth study of this new series of solid-state materials.

Compared with the electrocrystallization method reported in the literature,[13] a much simpler chemical method can be used to synthesize $[Ru(bpy)_3^{m+}]_n(C_{60}^{n-})_m$ in bulk. Electrochemical data on C_{60}^{n-} and $[Ru(bpy)_3]^{m+}$ in the format presented in Chart 1 were used as a guideline for establishing what oxidation states of C_{60} are compatible in solution with what Ru-complex oxidation states. Three possible accessible stoichiometries (n:m = 2:1, 1:1, and 1:2) were found. The reactions were carried out following Scheme 1. UV−vis−NIR, XPS, and elemental analyses were applied to determine the compositions of the bulk powder samples. Their single crystal structures and electronic properties are investigated and discussed in detail.

*To whom correspondence should be addressed. E-mail: elliott@lamar.colostate.edu.

(1) Konarev, D. V.; Khasanov, S. S.; Otsuka, A.; Saito, G.; Lyubovskaya, R. N. *CrystEngComm* **2009**, *11*, 811–816.
(2) Konarev, D. V.; Khasanovb, S. S.; Saitoc, G.; Lyubovskayaa, R. N. *J. Porphyrins Phthalocyanines* **2008**, *12*, 1146–1153.
(3) Domrachev, G. A.; Shevelev, Y. A.; Cherkasov, V. K.; Fukin, G. K.; Markin, G. V.; Kirillov, A. I. *Russ. Chem. Bull., Int. Ed.* **2006**, *55*, 225–229.
(4) Konarev, D. V.; Khasanov, S. S.; Kovalevsky, A. Y.; Saito, G.; Otsukae, A.; Lyubovskaya, R. N. *Dalton Trans.* **2006**, 3716–3720.
(5) Konarev, D. V.; Khasanov, S. S.; Saito, G.; Vorontsov, I. I.; Otsuka, A.; Lyubovskaya, R. N.; Antipin, Y. M. *Inorg. Chem.* **2003**, *42*, 3706–3708.
(6) Konarev, D. V.; Khasanov, S. S.; Vorontsov, I. I.; Saito, G.; Otsuka, A. *Synth. Met.* **2003**, *135*−*136*, 781–782.
(7) Konarev, D. V.; Khasanov, S. S.; Otsuka, A.; Saito, G. *J. Am. Chem. Soc.* **2002**, *124*, 8520–8521.
(8) Reed, C. A.; Bolskar, R. D. *Chem. Rev.* **2000**, *100*, 1075–1120.
(9) Konarev, D. V.; Khasanov, S. S.; Mukhamadieva, G. R.; Zorina, L. V.; Otsuka, A.; Yamochi, H.; Saito, G.; Lyubovskaya, R. N. *Inorg. Chem.* **2010**, *49*, 3881–3887.
(10) Boyd, P. D. W.; Bhyrappa, P.; Paul, P.; Stinchcombe, J.; Bolskar, R. D.; Sun, Y.; Reed, C. A. *J. Am. Chem. Soc.* **1995**, *117*, 2907–2914.
(11) Paul, P.; Xie, Z.; Bau, R.; Boyd, P. D. W.; Reed, C. A. *J. Am. Chem. Soc.* **1994**, *116*, 4145–4146.
(12) Elliott, C. M.; Hershenhart, E. J. *J. Am. Chem. Soc.* **1982**, *104*, 7519–7526.
(13) Foss, C. A., Jr.; Feldheim, D. L.; Lawson, D. R.; Dorhout, P. K.; Elliott, C. M.; Martin, C. R.; Parkinson, B. A. *J. Electrochem. Soc.* **1993**, *140*, L84–L86.
(14) Dresselhaus, M. S.; Dresselhaus, G.; Eklund, P. C. *Science of Fullerenes and Carbon Nanotubes*; Academic Press: New York, 1996.
(15) Biner, M.; Buergi, H. B.; Ludi, A.; Roehr, C. *J. Am. Chem. Soc.* **1992**, *114*, 5197–5203.
(16) Haddon, R. C. *Acc. Chem. Res.* **1992**, *25*, 127.

Published on Web 11/11/2010

Chart 1. Reductive Potential Regions of $[Ru(bpy)_3]^{m+}$ and C_{60}^{n-} Referenced to the Ferrocene/Ferrocenium Redox Couple[a]

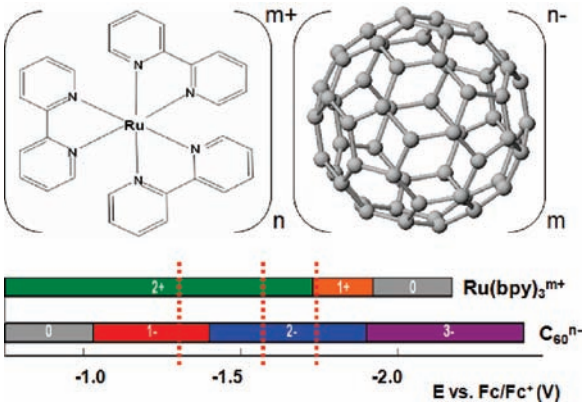

[a] Vertical lines separating different colored regions of the horizontal bars indicate the $E_{1/2}$ for the respective redox couple. For example, the $E_{1/2}$ for the $C_{60}^{0/-}$ couple is −1.03 V vs Fc/Fc^+. The colored bars indicate the charge borne by the dominant redox form of the complex within the potential range. Vertical dashed red lines represent potentials where the respective 1:2, 1:1, and 2:1 stoichiometries exist.

Experimental Section

General Procedures. C_{60} (≥99.5% purity) was purchased from Term-USA. 2,2′-bipyridine was supplied by Alfa Aesar. Ammonium hexafluorophosphate (Elf Atochem) and tetra-*n*-butylammonium hexafluorophosphate (electrochemical grade, Sigma Aldrich) were used as received. Benzonitrile (99%, Aldrich) was dried over sodium metal for 12 h and distilled under reduced pressure. Dry deoxygenated acetonitrile, *N*,*N*′-dimethylformamide (DMF), and toluene were obtained from a Pure-Solv solvent purification system. All solvents were stored in an inert atmosphere glovebox and were purged with N_2 gas prior to each use.

Visible/NIR spectra in solution were measured on a Cary 500 UV−vis−NIR spectrophotometer in a 1 mm airtight quartz cell. Solid-state transmission spectra were obtained in electronic absorption mode in KBr pressed pellet. Elemental analyses were performed at Robertson Microlit Laboratories, Inc., in Madison, NJ. The four-probe direct current (dc) conductivity was measured on thin pressed pellets of compounds supported on insulating KBr substrates. Details of the measurements and the apparatus are given in the Supporting Information, Figure S1. Single crystals suitable for X-ray diffraction were coated in Paratone oil prior to removal from inert atmosphere box, then glued to glass fibers, and mounted on a Bruker Kappa Apex 2 CCD diffractometer under N_2 stream. Data were collected using graphite-monochromatized Mo Kα radiation (λ = 0.71703 Å). Absorption corrections were performed with SADABS.[17] The structures were solved using the SHELXTL software package.[18] Electron paramagnetic resonance (EPR) spectra of solid samples were recorded on a Bruker X-band EPR spectrometer equipped with a temperature controller.

$[Ru(bpy)_3](PF_6)_2$. A modified literature procedure was used.[19] $Ru(DMSO)_4Cl_2$[20] (0.826 mmol) and 2,2′-bipyridine (2.56 mmol, 3.10 equiv) were combined in 30 mL of ethylene glycol and 8 mL of 1:1 CH_3OH:H_2O. The mixture was refluxed for 2 h in a 100 °C oil bath producing a clear red solution. An aqueous solution of NH_4PF_6 (1.84 mmol, 2.23 equiv) was added to the cooled solution whereupon a reddish orange precipitate immediately formed. After filtration, the solids were washed with H_2O and then a small amount of EtOH. Recrystallization from EtOH/acetone yielded red-orange crystals.

Scheme 1. Chemical Synthesis of Metal Complex Ionic C_{60} Salts

$$[Ru(bpy)_3]^{2+} \xrightarrow{2e^-} [Ru(bpy)_3]^0$$
$$2[Ru(bpy)_3]^0 + C_{60} \rightarrow [Ru(bpy)_3^{+}]_2(C_{60}^{2-})$$
$$[Ru(bpy)_3]^0 + C_{60} \rightarrow [Ru(bpy)_3^{2+}](C_{60}^{2-})$$
$$[Ru(bpy)_3]^0 + 2C_{60} \rightarrow [Ru(bpy)_3^{2+}](C_{60}^{-})_2$$

$[Ru(bpy)_3]^0$. Controlled-potential electrolytic reduction[21,22] was performed on $[Ru(bpy)_3](PF_6)_2$ in an inert atmosphere box to produce $[Ru(bpy)_3]^0$. A three compartment bulk electrolysis cell was used with Pt as counter electrode, Pt mesh as working electrode (W.E.), and Ag/Ag^+ 0.1 M in DMSO as reference electrode. The supporting electrolyte was 100 mM $TBAPF_6$ in CH_3CN. Prior to electrolysis, cyclic voltammetry was performed to determine the appropriate potential for reduction. For the specific reference electrode used, the maximum equilibrium concentration of $[Ru(bpy)_3]^0$ was obtained at −1.90 V. The W.E. was held at this potential until the measured coulombs passed matched the calculated value for the two-electron reduction of $[Ru(bpy)_3](PF_6)_2$. The $[Ru(bpy)_3]^0$ has limited solubility in acetonitrile and precipitated as a violet/black solid where it was collected from the Pt mesh electrode and washed with a few pipettes of fresh acetonitrile to remove excess supporting electrolyte. The washed solid was then dried by passing glovebox atmosphere over the solids with a vacuum suction. The oxidation state of the product was confirmed by comparison of the UV-visible spectrum with literature precedent.[12]

$[Ru(bpy)_3]_2(C_{60})$ (1). All manipulations were carried out in a glovebox filled with dinitrogen. $[Ru(bpy)_3]^0$ (40 mg, 0.070 mmol) was mixed with C_{60} (25.3 mg, 0.035 mmol) in 10 mL of benzonitrile. The solution color turned to reddish brown over 24 h of stirring followed by 30 min of ultrasonication at ambient temperature. Toluene (20 mL) was added to precipitate more solid. The solid was filtered, washed with toluene and then hexane, and dried under vacuum. X-ray photoelectron spectroscopy (Supporting Information, Figure S2) detected only trace amounts of phosphorus and fluorine which indicates that no significant amount of PF_6^- anion is incorporated into the ionic material. UV−vis−NIR spectra (Figure 1) showed evidence for $[Ru(bpy)_3]^{1+}$ (λ_{max} = 460 nm, 520 nm) and C_{60}^{2-} (λ_{max} = 958 nm).[12,23] The molar ratio between $[Ru(bpy)_3]^{1+}$ and C_{60}^{2-} was calculated from the spectrum to be 2.0 (±0.2): 1.0. Analysis for $C_{120}H_{48}N_{12}Ru_2$: Calcd C, 77.50; H, 2.58; N, 9.04. Found C, 77.22; H, 2.61; N, 8.89.

$[Ru(bpy)_3]_{1.07}(C_{60})\cdot 1.84(C_6H_5CN)$ (2). The compound was prepared the same way as **1** except a 1:1 molar ratio of $[Ru(bpy)_3]^0/C_{60}$ was used. The solution showed a sienna color. The presence of $[Ru(bpy)_3]^{2+}$ (λ_{max} = 422 nm, 458 nm) and C_{60}^{2-} (λ_{max} = 958 nm) were demonstrated in Figure 1.[12,23] The molar ratio calculated from the spectrum was 1.0 (±0.1):1.0. Analysis for $C_{90}H_{24}N_6Ru$ $\{[Ru(bpy)_3^{2+}](C_{60}^{2-})\}$: Calcd C, 83.78; H, 1.86; N, 6.51. Found C, 82.58; H, 2.29; N, 7.63. These elemental analysis data indicate that the "as-isolated" sample of **2** is not of single composition. To best fit the experimentally determined values, $[Ru(bpy)_3]_{1.07}(C_{60})\cdot 1.84(C_6H_5CN)$ was derived. Analysis for $C_{104.98}H_{34.88}N_{8.26}Ru_{1.07}$ $\{[Ru(bpy)_3]_{1.07}(C_{60})\cdot 1.84(C_6H_5CN)\}$: Calcd C,

(17) Sheldrick, G. M. *SADABS, A program for area detector absorption corrections*; Bruker AXS: Madison, WI.
(18) Sheldrick, G. *SHELXL-97 Program for Crystal Structure Refinement*; Bruker AXS: Madison, WI, 1997.
(19) Bloom, C. J.; Elliott, C. M.; Schroeder, P. G.; France, C. B.; Parkinson, B. A. *J. Phys. Chem. B* **2003**, *107*, 2933–2938.
(20) Evans, I. P.; Spencer, A.; Wilkinson, G. *J. Chem. Soc., Dalton Trans.* **1973**, 204–209.
(21) Pérez-Cordero, E. E.; Campana, C.; Echegoyen, L. *Angew.Chem., Int. Ed.* **1997**, *36*, 137–140.
(22) Pyo, S.; Perez-Cordero, E.; Bott, S. G.; Echegoyen, L. *Inorg. Chem.* **1999**, *38*, 3337–3343.
(23) Lawson, D. R.; Feldheim, D. L.; Foss, C. A.; Dorhout, P. K.; Elliott, C. M.; Martin, C. R.; Parkinson, B. *J. Electrochem. Soc.* **1992**, *139*, L68–L71.

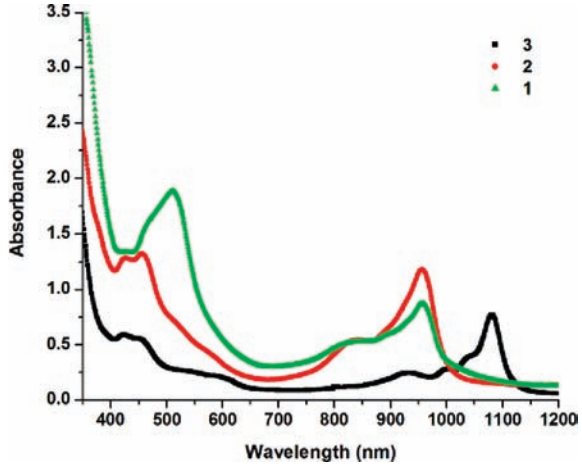

Figure 1. UV−vis−NIR absorption spectra of compounds **1**, **2**, and **3** in benzonitrile.

82.97; H, 2.30; N, 7.62. Found C, 82.58; H, 2.29; N, 7.63. $[Ru(bpy)_3]_{1.07}(C_{60})$ can be rewritten as $0.93[Ru(bpy)_3](C_{60})\cdot 0.07[Ru(bpy)_3]_2(C_{60})$. Because $[Ru(bpy)_3]^{1+}$ has a similar visible absorption spectrum to $[Ru(bpy)_3]^{2+}$, it would be difficult to identify the presence of minor amount of compound **1** from UV−vis−NIR spectrum. Also, the similar solubility of $[Ru(bpy)_3](C_{60})$ and $[Ru(bpy)_3]_2(C_{60})$ in most organic solvents makes the separation difficult. However, a single crystal of $[Ru(bpy)_3](C_{60})$ was successfully grown and analyzed starting from the "as-isolated" mixture.

$[Ru(bpy)_3](C_{60})_2$ (3). The procedure used was the same as that for **1** except the molar ratio of $[Ru(bpy)_3]^0/C_{60}$ was changed to 1:2. The solids dissolved in benzonitrile showed a goldenrod color. UV−vis−NIR spectra (Figure 1) showed characteristic absorption peaks for $[Ru(bpy)_3]^{2+}$ (λ_{max} = 422 nm, 458 nm) and C_{60}^- (λ_{max} = 1078 nm).[12,23] From the spectrum, the calculated molar ratio between cation and anion is 1.0 (±0.1): 2.0. Analysis for $C_{150}H_{24}N_6Ru$: Calcd C, 89.60; H, 1.19; N, 4.18. Found C, 89.20; H, 1.17; N, 4.58.

X-ray Crystal Structure Determination. Single crystals of $[Ru(bpy)_3^{1+}]_2(C_{60}^{2-})$ (**1′**) suitable for X-ray diffraction analysis were obtained by slow vapor diffusion of benzene into DMF at room temperature. Single crystals of $[Ru(bpy)_3^{2+}](C_{60}^{2-})$ (**2′**) were grown by slow vapor diffusion of toluene into benzonitrile at room temperature. Diffraction quality single crystals of **3** have not been obtained in part because of the poor solubility of the compound in most organic solvents. Details of crystallographic data for **1′** and **2′** are summarized in Table 1. Overall, the diffraction quality of crystal **2′** is much better than that of **1′**. Their asymmetric units are shown in the Supporting Information, Figure S3.

The Patterson method was applied for solving the crystal structure of **2′**. The space group of **2′** was determined to be centrosymmetric *C*2/*c*. The $[Ru(bpy)_3]^{2+}$ sits on a 2-fold rotation axis thus only 1.5 bpy ligands appear in the asymmetric unit. The C_{60}^{2-} also sits on the 2-fold rotation axis. A whole benzonitrile (C_6H_5CN) molecule sits on a general position. A toluene molecule sits on an inversion center, so the methyl group is disordered over two sites and was refined isotropically at 50% occupancy. However, another toluene molecule which sits on a 2-fold axis appears to be much more disordered. The thermal parameters for the latter toluene molecule were refined isotropically, and no H atoms were included for this badly disordered toluene (C_{57}−C_{62}). H atoms were calculated for all other C atoms, and the thermal parameters were set to be 1.2 times that of the attached carbon atoms except for 1.5 times that of the disordered methyl group on the first toluene.

For single crystal **1′**, much worse solvent disorder was observed. Also, there existed some disorder in the reduced C_{60}. The data was modified using SQUEEZE,[24] which implied approximately 0.75 equiv of DMF (per formula unit) are estimated to be present in the void space. The crystal structure was refined as centrosymmetric $R\,\bar{3}c$ with acceptable R_1 and wR_2 values.

Results and Discussion

Crystal Structures. In crystal **2′**, the mean values of 6−6 and 6−5 bonds in C_{60}^{2-} were found to be 1.396(5) Å and 1.449(5) Å. As compared to neutral C_{60} (a_6 = 1.40 Å, a_5 = 1.46 Å),[14] the 6−5 bond in particular is significantly shorter in C_{60}^{2-}. The diameter of C_{60}^{2-} anion was evaluated by measuring the distance of the two oppositely located carbon atoms. The longest diameter was measured to be 7.116 Å and the shortest one was 7.051 Å. The ellipsoidal deviation (~0.065 Å) is more than two times that for the parent C_{60} (0.025 Å).[25] As compared to other structurally determined C_{60}^{2-} salts with non-alkali or alkaline earth metal cations,[2,5,8,10,11,26−30] the moderate ellipsoidal deviation for C_{60}^{2-} in crystal **2′** is smaller than that in $(PPN)_2(C_{60})$ (0.086(5) Å) (PPN^+ = bis(triphenylphosphine) iminium ion),[11] but close to that in $(Cp^*_2Co)_2C_{60}\cdot(C_6H_4Cl_2, C_6H_5CN)_2$ (~0.06 Å) (Cp^*_2Co = decamethylcobaltocene)[5] and $[M(NH_3)_6]C_{60}\cdot 6NH_3$ (M = Ni, Mn) (0.0698 Å,[26] 0.0648 Å,[26,27] respectively). The addition of two electrons onto C_{60} greatly increases the distortion relative to neutral C_{60}. While it is probably inappropriate to make a detailed discussion about the bond lengths and angles in C_{60} of crystal **1′** because of crystallographic disorder, its crystal packing and interionic distances are still reliable.

The crystal packing of **1′** and **2′** projected on the *bc* plane is shown in Figure 2. It is obvious that in crystal **2′**, ions are well separated from each other. The nearest center-to-center distances of $C_{60}\cdots C_{60}$ and $(bpy)_3Ru\cdots Ru(bpy)_3$ are both 10.914(2) Å while the center-to-center distance of $(bpy)_3Ru\cdots C_{60}$ is shorter at 9.33(2) Å. The shortest carbon-to-carbon contact between $[Ru(bpy)_3]^{2+}$ and C_{60}^{2-} is 3.557(5) Å. In crystal **1′**, the C_{60} species are even farther apart. The nearest center-to-center distance is now 13.9063(2) Å. However, much shorter distances of $(bpy)_3Ru\cdots Ru(bpy)_3$ (8.1195(2) Å) and $(bpy)_3Ru\cdots C_{60}$ (8.8606(5) Å) are observed. The shortest carbon-to-carbon contact between $[Ru(bpy)_3]^{1+}$ and C_{60}^{2-} is 3.538(8) Å, while $[Ru(bpy)_3]C\cdots C[Ru(bpy)_3]$ distance is 3.45(3) Å. Comparing with K_3C_{60} [$C_{60}\cdots C_{60}$ = 10.06 Å, $(C_{60})C\cdots C(C_{60})$ = 3.01 Å],[14] both crystals show C_{60}^{2-} anions well separated from each other. However, in crystal **1′**, there is possible close contact between $[Ru(bpy)_3]^{1+}$ cations. The different interionic distances within crystal **1′** and **2′** potentially affect their electronic properties, which are discussed in detail below.

Magnetic Properties. The speciation of solid sample **1** and **3** is further confirmed by EPR spectra. (Considering

(24) Spek, A. L. *J. Appl. Crystallogr.* **2003**, *36*, 7–13.
(25) Bürgi, H.-B.; Blanc, E.; Schwarzenbach, D.; Liu, S.; Lu, Y.-j.; Kappes, M. M.; Ibers, J. A. *Angew. Chem., Int. Ed. Engl.* **1992**, *31*, 640–643.
(26) Himmel, K.; Jansen, M. *Chem. Commun.* **1998**, 1205–1206.
(27) Himmel, K.; Jansen, M. *Eur. J. Inorg. Chem.* **1998**, 1183–1186.
(28) Himmel, K.; Jansen, M. *Inorg. Chem.* **1998**, *37*, 3437–3439.
(29) Fässler, T. F.; Spiekermann, A.; Spahr, M. E.; Nesper, R. *Angew. Chem., Int. Ed. Engl.* **1997**, *36*, 486–488.
(30) Himmel, K.; Jansen, M. *Z. Anorg. Allg. Chem.* **1998**, *624*, 1–3.

Table 1. Crystallographic Data for **1′** and **2′**

	1′	**2′**
empirical formula	$C_{150}H_{102}N_{18}O_6Ru_2$	$C_{118}H_{42}N_8Ru$
structural formula	$[Ru(bpy)_3]_2\cdot(C_{60})\cdot(C_3H_7NO)_6\cdot(C_6H_6)_2$	$Ru(bpy)_3\cdot(C_{60})\cdot(C_6H_5CN)_2\cdot(C_7H_8)\cdot C_7$
formula weight ($g\cdot mol^{-1}$)	2454.64	1672.67
D_{calc} ($g\cdot cm^{-3}$)	1.474	1.477
temperature (K)	100(2)	100(2)
crystal system	trigonal	monoclinic
space group	$R\bar{3}c$	$C2/c$
a (Å)	13.9063(2)	10.914(2)
b (Å)	13.9063(2)	40.612(8)
c (Å)	99.067(3)	17.303(4)
α (deg)	90.00	90.00
β (deg)	90.00	101.17(3)
γ (deg)	120.00	90.00
V (Å^3)	16591.3(6)	7524(3)
Z	6	4
unique reflections	4592	8743
R (int)	0.0628	0.0357
parameters	267(0)	561(0)
$F(000)$	7584	3400
$2\theta_{max}$ (deg)	56.56	56.56
resolution (Å)	0.75	0.75
GOF	1.092	1.045
$R_1{}^a$ [$F_o > 4\sigma(F_o)$]	0.0812	0.0548
$wR_2{}^b$	0.2200	0.1530

$^a R_1 = \sum||F_o| - |F_c||/\sum|F_o|$. $^b wR_2 = \{\sum[w(F_o^2 - F_c^2)^2]/\sum[w(F_o^2)^2]\}^{1/2}$.

the multicomposition of sample **2**, EPR data is not included here.) According to many previous reports in the literature, instead of having a triplet ground state ($S = 1$), $C_{60}{}^{2-}$ prefers a singlet ground state ($S = 0$) with only a small portion of close-lying triplet excited states ($S = 1$) because of the Jahn−Teller distortion of the dianion.[8,31−36] Therefore, in compound **1**, the dominant contribution of the observed EPR signal originates from the unpaired electrons on $[Ru(bpy)_3]^{1+}$ ($S = 1/2$).[37] At 292 K, a single broad line with $g = 1.9999$ (±0.0002) was observed (Figure 3). Cooling down to 105 K, the signal becomes stronger with narrower line width. The temperature dependence of the EPR signal for compound **1** is consistent with that of the EPR spectra for $[Ru(bpy)_3]^{1+}$ reported previously.[38] In compound **3**, $C_{60}{}^-$ ($S = 1/2$) is EPR active while $[Ru(bpy)_3]^{2+}$ is not ($S = 0$).[8,37] In Figure 4, a characteristic broad signal of $C_{60}{}^-$ was observed with $g = 2.0014$ (±0.0002) at 292 K.[35] The peak-to-peak line width decreases from 4 mT to 2 mT as the temperature is lowered from 292 to 100 K, which can be explained by the slower electron spin−lattice relaxation at lower temperature.[35]

The temperature dependencies of the magnetic susceptibility for compounds **1** and **3** are complex (Supporting Information, Figures S4 and S5). The compounds do not show Curie−Weiss behavior, indicating that the compounds do not contain magnetically isolated spin centers. Weak antiferromagnetic coupling between spins is inferred based on the tendency for the systems to display diamagnetic ground states at low temperatures. More details are included in the Supporting Information.

Electrical Conductivity. At room temperature, all three compounds show absolute conductivities in the semiconductor range (Table 2).[39] As the temperature increases, their conductivities increase as well. The order for descending conductivity is **1** > **3** > **2**. Compound **1** is about 500 times more conductive than **2**, while **3** is about 100 times more conductive than **2**. On the basis of the result of elemental analysis, compounds **1** and **3** correspond to $[Ru(bpy)_3]_2(C_{60})$ and $[Ru(bpy)_3](C_{60})_2$ respectively, while compound **2** is mainly $[Ru(bpy)_3](C_{60})$ with a small amount of compound **1** $[Ru(bpy)_3]_2(C_{60})$. Because of the relatively high conductivity of compound **1**, the pure form of compound **2** should exhibit conductivity even smaller than $0.018\ S\ m^{-1}$. Since this does not conflict with the observed trend of conductivity, the following discussion will be based on the assumption that compound **2** is pure with formula $[Ru(bpy)_3](C_{60})$.

In the single crystal structures of **1′** and **2′**, there is only weak site−site interaction since the cations and anions are all well separated from each other. The electronic conductivity is best described by an electron hopping model in this immobilized polyvalent redox system rather than by a band structure.[40,41]

There are two limiting factors for electron hopping efficiency.[42] The first is the relative concentrations of electron hopping sites, which greatly depend on the degree of mixed-valency.[42] Increasing the relative number of electron donors and acceptors increases the probability of charge transport.[42,43] For $[Ru(bpy)_3]_n(C_{60})_m$ compounds, both cation and anion are, in principle, electroactive. Supposing the respective stoichiometries of compound **1**, **2**, and **3**, distribution of various redox species in solution at equilibrium can be calculated from the Nernst equation and the electroneutrality principle (Table 2). For qualitative discussion, disproportionation calculated in solution can serve as a reasonable approximation for the case in solid state but is almost certainly not quantitatively the same. Possible electron hopping pathways are predicted in Scheme 2. Obviously, among the three, **1** has the highest degree of mixed-valency and the maximum number of possible electron transfer pathways.

The second important factor in determining the operative electron-hopping pathways is the intersite hopping distance.[42] The overlap of the highest occupied molecular orbital (HOMO) and the lowest unoccupied molecular

(31) Bhyrappa, P.; Paul, P.; Stinchcombe, J.; Boyd, P. D. W.; Reed, C. A. *J. Am. Chem. Soc.* **1993**, *115*, 11004–11005.
(32) Saito, R.; Dresselhaus, G.; Dresselhaus, M. S. *Chem. Phys. Lett.* **1993**, *210*, 159–164.
(33) Dubois, D.; Jones, M. T.; Kadish, K. M. *J. Am. Chem. Soc.* **1992**, *114*, 6446–6451.
(34) Trulove, P. C.; Carlin, R. T.; Eaton, G. R.; Eaton, S. S. *J. Am. Chem. Soc.* **1995**, *117*, 6265–6272.
(35) Eaton, S. S.; Eaton, G. R. *Appl. Magn. Reson.* **1996**, *11*, 155–170.
(36) Negri, F.; Orlandi, G.; Zerbetto, F. *J. Am. Chem. Soc.* **1992**, *114*, 2909–2913.
(37) Morris, D. E.; Hanck, K. W.; DeArmond, M. K. *J. Am. Chem. Soc.* **1983**, *105*, 3032–3038.
(38) Motten, A. G.; Hanck, K.; DeArmound, M. K. *Chem. Phys. Lett.* **1981**, *79*, 541–546.
(39) Single crystals of **1**−**3** should exhibit anisotropic conductivity; thus it would be highly desirable to make four-probe conductivity measurements along different crystal axes. However, despite significant efforts on our part, we were unable to grow crystals which were large enough to attempt such measurements.
(40) Murray, R. W. *Electroanal. Chem.* **1984**, *13*, 191–368.
(41) Murray, R. W. *Annu. Rev. Mater. Sci.* **1984**, *14*, 145–169.
(42) Baldy, C. J.; Elliott, C. M.; Feldberg, S. W. *J. Electroanal. Chem.* **1990**, *283*, 53–65.
(43) Saveant, J.-M. *J. Phys. Chem.* **1988**, *92*, 1011–1013.

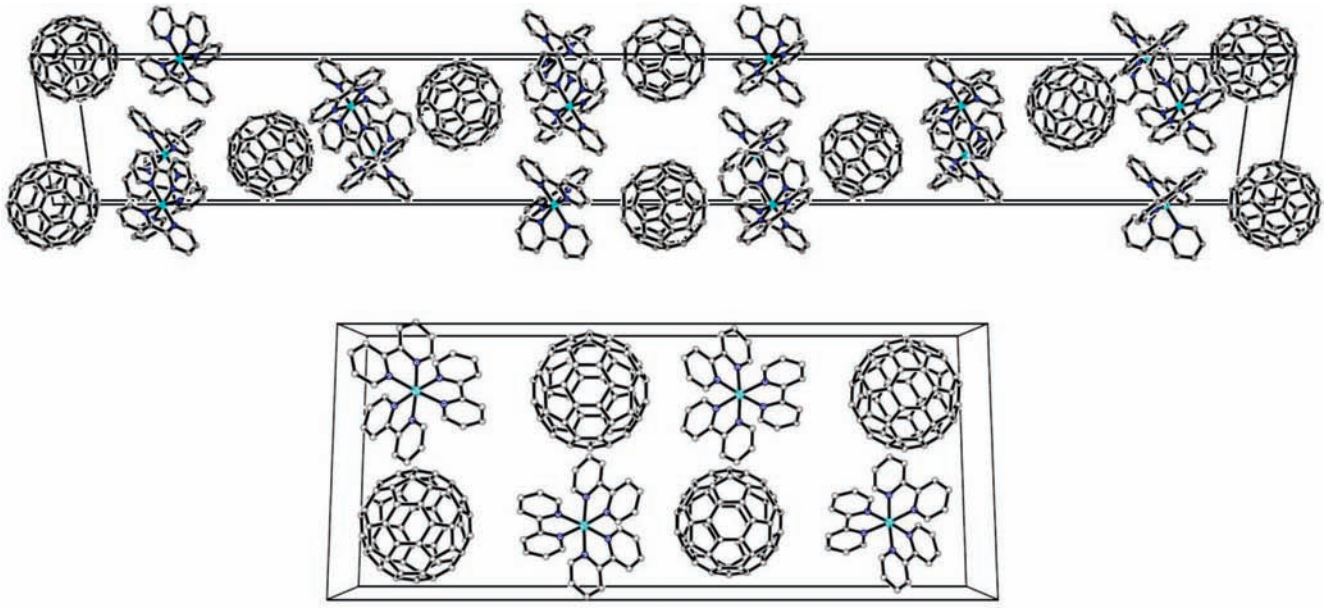

Figure 2. Projection of the crystal packing of **1′** (top) and **2′** (bottom) on the *bc* plane. The solvent molecules were omitted for clarity.

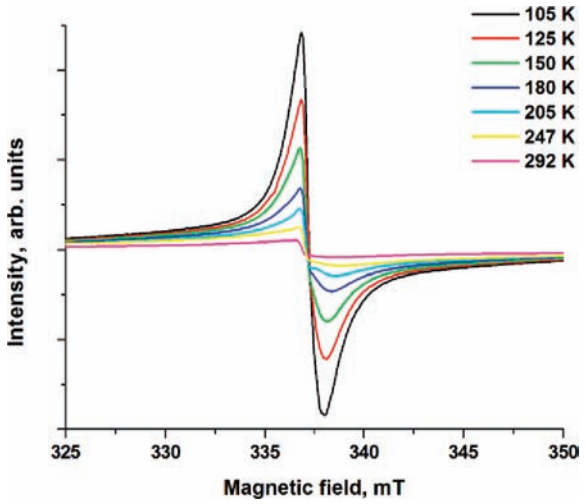

Figure 3. EPR spectra of solid sample **1** at temperatures ranging from 292 to 105 K.

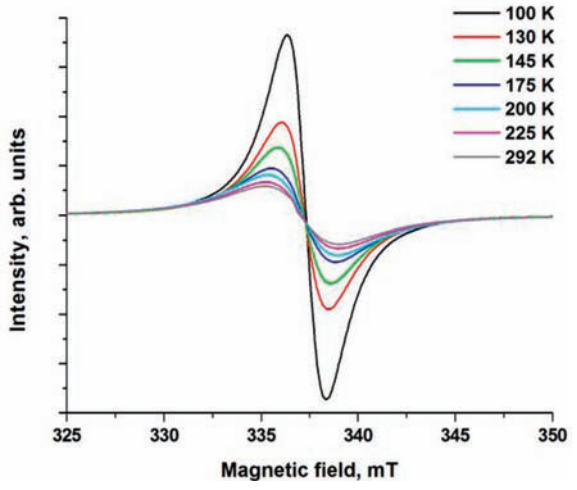

Figure 4. EPR spectra of solid sample **3** at temperatures ranging from 292 to 100 K.

orbital (LUMO) of electron donor and acceptor decreases as the distance increases, which results in a higher activation energy for an electron to hop. Therefore, shorter site−site distance generally should result in easier electron hopping. For crystals **1′** and **2′**, the positions and surroundings of $[Ru(bpy)_3]^{m+}$ and C_{60}^{n-} sites are included in the Supporting Information, Figures S6−S9. In single crystal **2′**, $[Ru(bpy)_3]^{m+}$ and C_{60}^{n-} basically occupy the interchangeable positions in the unit cell. There are two types of $[Ru(bpy)_3]^{m+}$ (or C_{60}^{n-}) sites with different surroundings. Both types represent the shortest center-to-center distance (9.33(2) Å) between adjacent $[Ru(bpy)_3]^{m+}$ and C_{60}^{n-} on the *ac* plane. And the second shortest distance (10.69(19) Å) is between adjacent $[Ru(bpy)_3]^{m+}$ and C_{60}^{n-} along the *b* axis. In single crystal **1′**, three types of $[Ru(bpy)_3]^{m+}$ sites as well as two types of C_{60}^{n-} sites were found. The shortest site−site distance is 8.1195(2) Å between adjacent $[Ru(bpy)_3]^{m+}$ sites on the *ab* plane. The second shortest distance turned out to be 8.8606(5) Å between the neighboring $[Ru(bpy)_3]^{m+}$ and C_{60}^{n-} along the *c* axis. Apparently, longer intersite distances were found in the single crystal **2′** and thus it will be harder for electrons to hop from one site to another as compared to those in the single crystal **1′**. The indication from structural information is in accordance with the conductivity results that compound **1** is much more conductive than compound **2**. As for compound **3**, the electron transfers exclusively reside in the C_{60} manifold while $[Ru(bpy)_3]^{2+}$ only act as a spacer (Scheme 2). Because the electrons only hop from one C_{60} to another, the $C_{60}\cdots C_{60}$ distances are of more importance for conductivity than other site−site distances. When the degree of mixed-valency and number of electron-transfer pathways are similar in **2** and **3**, the fact that **3** is about 100 times more conducting than **2** might be explained by

Table 2. Electrical Conductivities of Compounds **1**−**3** at Room Temperature and the Calculated Distribution of Redox Species in Solution at Room Temperature[a]

compound	σ (S m^{-1})	RuL_3^{2+}	RuL_3^{1+}	RuL_3^{0}	C_{60}	C_{60}^{-}	C_{60}^{2-}	C_{60}^{3-}
1	**9.5** (±26%)	0.068	1.900	0.032	0	0	0.964	0.036
2	**0.018** (±13%)	0.998	0.002	0	0	0.002	0.998	0
3	**2.0** (±31%)	1.000	0	0	0.0015	1.997	0.0015	0

[a] L represents 2,2′-bipyridine ligand.

Scheme 2. Schematic Pictures of Possible Electron Transfer in Compound **1** (**a**), **2** (**b**), and **3** (**c**)[a]

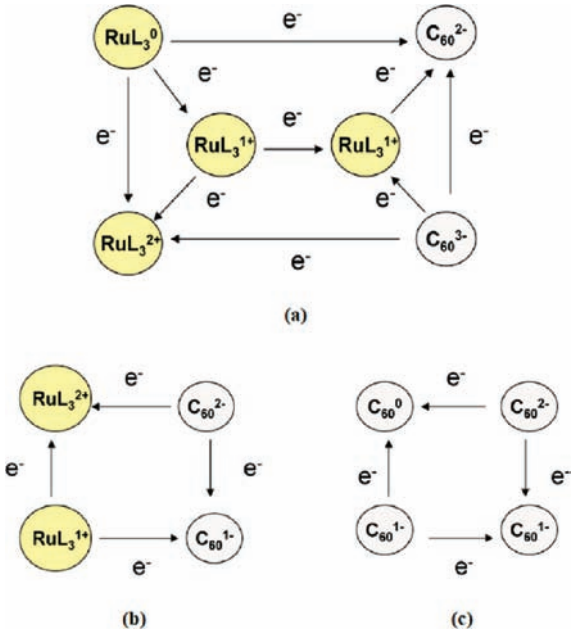

[a] L represents 2,2′-bipyridine ligand.

the easier electron hopping in **3** because of its possible shorter $C_{60}\cdots C_{60}$ distances. Based in Scheme 2, all possible electron transfer mechanisms for all three compounds are listed in Table 3. Combining the conclusions from analyzing intersite distances in compounds **1**, **2**, and **3** with their mixed-valency information, the favorable electron hopping pathway can be predicted as follows.

In compound **1**, there are nine possible electron-transfer mechanisms, which fall into three groups. Group I includes the following four equations.

$$RuL_3^{+} + RuL_3^{+} \rightleftharpoons RuL_3^{2+} + RuL_3^{0} \qquad (1\text{-}1)$$

$$RuL_3^{0} + RuL_3^{2+} \rightleftharpoons RuL_3^{+} + RuL_3^{+} \qquad (1\text{-}6)$$

$$RuL_3^{+} + C_{60}^{2-} \rightleftharpoons RuL_3^{2+} + C_{60}^{3-} \qquad (1\text{-}3)$$

$$C_{60}^{3-} + RuL_3^{2+} \rightleftharpoons C_{60}^{2-} + RuL_3^{+} \qquad (1\text{-}9)$$

Consider first reaction 1-6, where the relative concentrations calculated from solution redox data of RuL_3^{0}, RuL_3^{2+}, and RuL_3^{1+} are 0.032, 0.068, and 1.900, respectively (Table 2). For the electron to hop via this mechanism, one RuL_3^{0} and one RuL_3^{2+} must happen to sit on the adjacent positions. Considering their small relative concentrations and assuming a random distribution over the solids, the probability that this electron hop is a major contribution to the overall conduction would be very small. Therefore, eq 1-6 is not likely to be an important electron hopping mechanism. Reaction 1-9 is also unfavorable for the same reasons. (Concentrations of reactants C_{60}^{3-} and RuL_3^{2+} are only 0.036 and 0.068.) Reactions 1-1 and 1-3 are simply the reverse of 1-6 and 1-9. Although here both reactants have large concentrations, the probability of generating two minor species would be small for thermodynamic reasons. On the whole, the first group of mechanism 1-1, 1-3, 1-6, and 1-9 is considered as "unfavorable" in their contributions to the hopping. In group II, three "favorable" mechanisms for electron transfer were found.

$$RuL_3^{+} + RuL_3^{2+} \rightleftharpoons RuL_3^{2+} + RuL_3^{+} \qquad (1\text{-}2)$$

$$RuL_3^{0} + RuL_3^{+} \rightleftharpoons RuL_3^{+} + RuL_3^{0} \qquad (1\text{-}4)$$

$$C_{60}^{3-} + C_{60}^{2-} \rightleftharpoons C_{60}^{2-} + C_{60}^{3-} \qquad (1\text{-}7)$$

The similarity of all three above equations is that the reactants and products are the same. Thus, since the equilibrium constant for each reaction equals 1, the thermodynamic "cost" is zero (ignoring, of course, any coulombic contribution to rearrange charges within the solid). Also, the presence of at least one ion present at high relative concentration on the reactant side greatly increases the probability of electron hopping. Contribution from reactions in the third group (shown below) is less clear.

$$RuL_3^{0} + C_{60}^{2-} \rightleftharpoons RuL_3^{+} + C_{60}^{3-} \qquad (1\text{-}5)$$

$$C_{60}^{3-} + RuL_3^{+} \rightleftharpoons C_{60}^{2-} + RuL_3^{0} \qquad (1\text{-}8)$$

On the basis of the concentration given in Table 2, the K_{eq} for 1-5 and 1-8 are calculated to be 2.22 and 0.45, respectively. Also, each reaction involves one reactant that is present at a large relative concentration. Thus, while they are not thermoneutral processes, their contribution to the overall conduction mechanism cannot be discounted.

Combining the above discussion with the site−site distribution information obtained from X-ray diffraction of compound **1**, the most preferable electron hopping mechanisms can be predicted as follows with site−site distance 8.1195(2) Å along the *ab* plane.

$$RuL_3^{0} + RuL_3^{+} \rightleftharpoons RuL_3^{+} + RuL_3^{0}$$

$$RuL_3^{+} + RuL_3^{2+} \rightleftharpoons RuL_3^{2+} + RuL_3^{+}$$

Table 3. Prediction of Possible Electron Hopping Mechanism in Compounds **1**, **2**, and **3**[a]

compound	possible pathways		favorable (F) or unfavorable (UF)
1	$RuL_3^{+} + RuL_3^{+} \rightharpoonup RuL_3^{2+} + RuL_3^{0}$	(1−1)	UF
	$RuL_3^{+} + RuL_3^{2+} \rightharpoonup RuL_3^{2+} + RuL_3^{+}$	(1−2)	F
	$RuL_3^{+} + C_{60}^{2-} \rightharpoonup RuL_3^{2+} + C_{60}^{3-}$	(1−3)	UF
	$RuL_3^{0} + RuL_3^{+} \rightharpoonup RuL_3^{+} + RuL_3^{0}$	(1−4)	F
	$RuL_3^{0} + C_{60}^{2-} \rightharpoonup RuL_3^{+} + C_{60}^{3-}$	(1−5)	F (possible)
	$RuL_3^{0} + RuL_3^{2+} \rightharpoonup RuL_3^{+} + RuL_3^{+}$	(1−6)	UF
	$C_{60}^{3-} + C_{60}^{2-} \rightharpoonup C_{60}^{2-} + C_{60}^{3-}$	(1−7)	F
	$C_{60}^{3-} + RuL_3^{+} \rightharpoonup C_{60}^{2-} + RuL_3^{0}$	(1−8)	F (possible)
	$C_{60}^{3-} + RuL_3^{2+} \rightharpoonup C_{60}^{2-} + RuL_3^{+}$	(1−9)	UF
2	$RuL_3^{+} + RuL_3^{2+} \rightharpoonup RuL_3^{2+} + RuL_3^{+}$	(2−1)	F
	$RuL_3^{+} + C_{60}^{-} \rightharpoonup RuL_3^{2+} + C_{60}^{2-}$	(2−2)	UF
	$C_{60}^{3-} + C_{60}^{2-} \rightharpoonup C_{60}^{2-} + C_{60}^{3-}$	(2−3)	F
	$C_{60}^{2-} + RuL_3^{2+} \rightharpoonup C_{60}^{-} + RuL_3^{+}$	(2−4)	UF
3	$C_{60}^{-} + C_{60}^{0} \rightharpoonup C_{60}^{0} + C_{60}^{-}$	(3−1)	F
	$C_{60}^{-} + C_{60}^{-} \rightharpoonup C_{60}^{0} + C_{60}^{2-}$	(3−2)	UF
	$C_{60}^{2-} + C_{60}^{-} \rightharpoonup C_{60}^{-} + C_{60}^{2-}$	(3−3)	F
	$C_{60}^{2-} + C_{60}^{0} \rightharpoonup C_{60}^{-} + C_{60}^{-}$	(3−4)	UF

[a] L represents 2,2′-bipyridine ligand.

The same protocol was followed to predict the favorable and unfavorable electron hopping pathways in compounds **2** and **3** (Table 3).

In the single crystal of **2**, electrons would prefer the following two hopping pathways with site−site distance in each case of 10.914(2) Å along the *a* axis.

$$RuL_3^{+} + RuL_3^{2+} \rightleftharpoons RuL_3^{2+} + RuL_3^{+}$$

$$C_{60}^{3-} + C_{60}^{2-} \rightleftharpoons C_{60}^{2-} + C_{60}^{3-}$$

In compound **3**, electrons can only transfer between C_{60} species, and they should prefer to hop between C_{60} species that differ by one unit charge difference.

$$C_{60}^{-} + C_{60}^{0} \rightleftharpoons C_{60}^{0} + C_{60}^{-}$$

$$C_{60}^{2-} + C_{60}^{-} \rightleftharpoons C_{60}^{-} + C_{60}^{2-}$$

To our knowledge, this is the first attempt to correlate structural parameters and solid-state mixed valency with electronic conductivity for metal-complex ionic fullerene salts. Most of the other structurally determined metal-complex ionic C_{60}^{2-} salts contain cations that are redox-inert over the potential region where C_{60} is redox-active.[8,10,26−29] Therefore, in most cases, only C_{60}^{n-} participates in the electron conduction and thus only the $C_{60}\cdots C_{60}$ interactions are of consequence. Other metal-complex C_{60}^{2-} salts in literature showed for C_{60}-(C)$\cdots$(C)C_{60} a wide range of intermolecular distances, the shortest being 3.36 Å in $[Ni(NH_3)_6](C_{60})$.[26] In our most conductive compound, $[Ru(bpy)_3]_2(C_{60})$, the shortest electron hopping pathway is between adjacent $Ru(bpy)_3$ cations with a distance $[Ru(bpy)_3]C\cdots C[Ru(bpy)_3]$ = 3.45(3) Å. Of the structurally determined metal-complex ionic C_{60}^{2-} salts previously reported, a few have possible contributions from the cation to the conductivity.[2,5] Unfortunately, in case where the cation is a metalloporphyrin, the solid-state redox potentials are much less well-defined because of the sensitivity of the redox chemistry of the porphyrin to axial substituents; thus it is difficult to know the extent that the cation participates in the conduction mechanism. One prior example where the redox properties of the cation are well-defined is $[Cp^*_2Co]_2(C_{60})$.[5] However, in this case, only a very small degree of mixed-valency is expected in solid $[Cp^*_2Co]_2(C_{60})$ (< 0.006%) compared to > 0.2% for $[Ru(bpy)_3]_n(C_{60})_m$. At least for compound **1** and **2**, the conductivity of $[Ru(bpy)_3]_n(C_{60})_m$ salts are consistent with the participation of redox-active cations in the electronic conduction and the relatively short intersite electron hopping distances.

Finally, given the mixed-valence nature of these materials, one might anticipate new optical bands to be present in the solid-state spectra (because of charge-transfer transitions) that are absent in dilute solution spectra. Transmission spectra were thus obtained on solid samples of **1**−**3** in pressed KBr pellets and compared with the corresponding solution spectra (Supporting Information, Figure S10). While there are differences evident between solution and solid-state spectra, no new bands are discernible in the latter which could be attributed to charge-transfer transitions. Given the fairly congested nature of the spectra across the entire vis−NIR region and the relatively small degree of mixed valency, this is not especially surprising. In other words, CT-type transitions might be present which are simply too weak to see under the experimental conditions employed.

Conclusions

The three $[Ru(bpy)_3]_n(C_{60})_m$ salts investigated herein are semiconductors in both temperature-dependence

and absolute conductivity. The mechanism of conductivity is best rationalized from an electron hopping model where the relative concentrations of electron donor and acceptor sites and hopping distance are both taken into account. Within these materials, the donor and acceptor sites are generated by disproportionations of the redox-active ions in the solid state and result in multispecies mixed valency. The solution redox potentials serve as useful guides to identify which species are most likely to contribute in the electron-transport process. In general (and in contrast to alkali metal fullerides), potentially important electron conduction pathways can be identified along the anion manifold, the cation manifold, or both. Moreover, as in the case of **1**, additional pathways may be important which cross between the cation/anion manifolds. The X-ray structural data provide important insights about hopping distances and pathways and show that these materials lack the extended three-dimensional $C_{60}-C_{60}$ close contacts characteristic of the alkali-metal salts.

Acknowledgment. We gratefully acknowledge support of this work through a grant from the National Science Foundation (CHE-0139635 for C.M.E., J.H.) and from Colorado State University (for M.P.S.).

Supporting Information Available: X-ray crystallographic data in CIF format. Design of four-probe conductivity measurements (Figure S1). XPS spectra (Figure S2). Asymmetric units of crystal **1′** and **2′** (Figure S3). Magnetic susceptibility data for compounds **1** and **3** (Figures S4−S5). Surroundings of $[Ru(bpy)_3]^{m+}$ sites and C_{60}^{n-} sites in single crystal **1′** and **2′** (Figures S6−S9). Solid-state visible/NIR spectra (Figure S10). Equations for calculating relative concentrations of disproportionated redox species (Tables S1−S3). This material is available free of charge via the Internet at http://pubs.acs.org.